

Microcavity-enhanced surface-emitted second-harmonic generation from 200 fs pulses at 1.5 μm

Todd G. Ulmer, Marc Hanna, Brian R. Washburn, Carl M. Verber, and Stephen E. Ralph^{a)}
*School of Electrical and Computer Engineering, Georgia Institute of Technology, Atlanta,
 Georgia 30332-0250*

Anthony J. SpringThorpe
Nortel Networks Microelectronics, Ottawa, Ontario, Canada, K2H 8E9

(Received 2 February 2001; accepted for publication 4 April 2001)

We present theoretical results for short-pulse surface-emitted second-harmonic generation and show that significant cavity enhancement is possible in the femtosecond regime. Experimentally, we demonstrate enhanced surface-emitted second-harmonic generation using 200 fs fundamental pulses near 1.5 μm by use of a $5\lambda^{\text{SH}}/2n$ vertical microcavity in [211]-oriented AlGaAs waveguides. The microcavity height is minimized by allowing the distributed Bragg reflectors that define the vertical cavity to also serve as cladding layers for the fundamental waveguide, thereby increasing the resonance width and hence the overlap with the second-harmonic spectrum. © 2001 American Institute of Physics. [DOI: 10.1063/1.1376429]

Surface-emitted second-harmonic generation (SESHG) provides a means for ultrafast all-optical signal processing made possible by the colliding-pulse surface-emitting geometry. Indeed, optical serial-to-parallel conversion for time-division demultiplexing has been demonstrated.^{1,2} The colliding-pulse geometry, however, limits the optical interaction length and hence the conversion efficiency. Resonant cavity enhancement of SESHG via a vertical microcavity has previously been shown to increase the efficiency by up to two orders of magnitude in the quasi-cw regime,³⁻⁵ where the spectral content of the nonenhanced second harmonic (SH) is narrow compared to the resonance width of the cavity. However, we find that significant enhancement is possible even for subpicosecond pulses, where the spectral content exceeds the resonance width of the microcavity. The enhancement afforded by an appropriate microcavity can enable ultrafast optical time-division demultiplexing in the important 1.5 μm wavelength region. Here, we report theoretical and experimental results of the SESHG efficiency for 200 fs fundamental pulses in a $5\lambda^{\text{SH}}/2n$ AlGaAs microcavity.

We begin with a theoretical description of short-pulse SESHG. The total SH is determined via the product of the base efficiency and a frequency-dependent enhancement fac-

tor due to the resonant cavity. The base efficiency is calculated using a Green's function approach which allows the determination of the single-pass SH from arbitrary nonlinear source terms.^{6,7} We assume transverse electric (TE)-polarized fundamental fields in [211]-oriented material for optimum efficiency in AlGaAs.⁸ The complex amplitude of the SH electric field emitted toward the surface in the absence of a microcavity is

$$E_x^{\text{SH}}(z) = \int_{-\infty}^z \frac{-ik}{2\epsilon} P_{\text{NL}}(z') \exp\left(-i \int_{z'}^z k(z'') dz''\right) dz', \quad (1)$$

where $P_{\text{NL}}^{[211]}(z) = 4/\sqrt{3} \epsilon_0 d_{14}(z) E_+^{(\omega)}(z) E_-^{(\omega)}(z)$ is the spatially dependent nonlinear polarization, k is the wave number, $\epsilon = \epsilon_r \epsilon_0$ is the permittivity, and $E_+^{(\omega)}$ and $E_-^{(\omega)}$ are the counter-propagating electric field strengths. The second integral accounts for the phase accumulation of the wave emitted by each source term to the top of the structure.

The frequency-dependent cavity-enhancement factor is separately determined by calculating the total field outside the cavity resulting from a single plane-wave source within the cavity⁹ that emits equally in both directions.¹⁰ The resulting enhancement factor is

$$\frac{P_t^{\text{SH}}(\omega)}{P_0^{\text{SH}}(\omega)} = (1 - |r_t|^2) \frac{(1 + |r_b| e^{-\alpha l})^2 - 4|r_b| e^{-\alpha l} \sin^2\left(kl - \frac{\phi_b}{2}\right)}{(1 - |r_t||r_b| e^{-\alpha d})^2 + 4|r_t||r_b| e^{-\alpha d} \sin^2\left(kd - \frac{\phi_t}{2} - \frac{\phi_b}{2}\right)}, \quad (2)$$

where $P_t^{\text{SH}}(\omega)$ is the SH power emitted through the top mirror, $P_0^{\text{SH}}(\omega)$ is the SH power emitted toward the surface in the absence of a microcavity, $r_b = |r_b| \exp(i\phi_b)$ is the field

reflectivity of the bottom mirror, r_t is the reflectivity of the top mirror, α is the absorption coefficient, l is the distance from the source to the bottom mirror, and d is the cavity mirror separation. The frequency dependence of the enhancement factor is contained in the wave number $k = \omega^{\text{SH}} n/c$ and

^{a)}Electronic mail: stephen.ralph@ece.gatech.edu

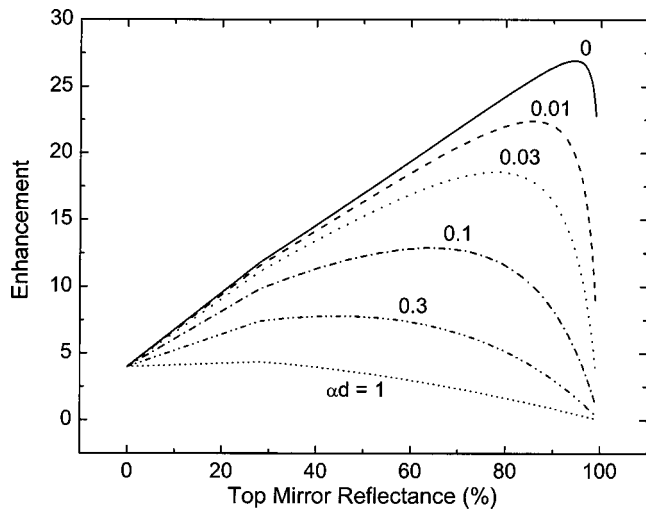


FIG. 1. Calculated SESHG enhancement for 200 fs fundamental pulses in a $5\lambda^{\text{SH}}/2n$ vertical microcavity as a function of top mirror reflectance and intracavity loss. The bottom mirror reflectance is fixed to 99.7%.

in the complex mirror reflectivities. Cavity resonances occur at frequencies where the round-trip phase shift in the cavity, given by $2kd - \phi_t - \phi_b$, is an integral multiple of 2π . The net enhancement is obtained by integration $\Gamma = \int P_t^{\text{SH}}(\omega) d\omega / \int P_0^{\text{SH}}(\omega) d\omega$. Figure 1 depicts the net enhancement versus the top mirror reflectance for a $5\lambda^{\text{SH}}/2n$ cavity and a 200 fs fundamental pulse. Incorporating high reflectance and low absorption allows enhancements greater than 20.

In the short-pulse regime, the cavity significantly modifies the temporal characteristics of the SH pulse. Therefore, it is useful to describe the efficiency in terms of pulse energies to facilitate comparison with experiment. The base nonlinear cross section for Gaussian pulses is

$$A_0^{\text{NL}} = \frac{w^{(\omega)} w^{(\omega)} \mathcal{E}^{\text{SH}} 2\xi}{\mathcal{E}_+^{(\omega)} \mathcal{E}_-^{(\omega)} w^{\text{SH}} v_g}, \quad (3)$$

where \mathcal{E}^{SH} is the SH pulse energy, $\mathcal{E}_{\pm}^{(\omega)}$ are the counter-propagating fundamental pulse energies, v_g is the group velocity, $w^{(\omega)}, w^{\text{SH}}$ are the widths of the fundamental modes and the SH beam, respectively, and $\xi = \sqrt{\pi/4 \ln 2}$ is a factor relating peak power and temporal width to energy. Inclusion of the cavity effects yields an effective cross section $A_{\text{eff}}^{\text{NL}} = A_0^{\text{NL}} \Gamma$.

For our calculations, we estimate the second-order nonlinear optical coefficients using the recently reported absolute value for GaAs,¹¹ $d_{14} = 119$ pm/V at $1.533 \mu\text{m}$. Assuming the compositional dependence reported in Ref. 7 remains valid at $1.5 \mu\text{m}$, we estimate $d_{14} = 73$ pm/V for $\text{Al}_{0.30}\text{Ga}_{0.70}\text{As}$ and 18 pm/V for $\text{Al}_{0.90}\text{Ga}_{0.10}\text{As}$. We note that these values are significantly lower than those commonly cited.

The multilayer AlGaAs waveguide structure includes a five-layer quasi-phase-matched (QPM) waveguide core incorporated between two distributed Bragg reflectors (DBRs). The structure is comprised of a 35 period $\text{Al}_{0.45}\text{Ga}_{0.55}\text{As}/\text{AlAs}$ bottom DBR ($R = 99.7\%$), a 2.5 period $\text{Al}_{0.30}\text{Ga}_{0.70}\text{As}/\text{Al}_{0.90}\text{Ga}_{0.10}\text{As}$ QPM waveguide core, and a 19.5 period $\text{Al}_{0.45}\text{Ga}_{0.55}\text{As}/\text{Al}_{0.90}\text{Ga}_{0.10}\text{As}$ top DBR ($R = 94.8\%$). By allowing the DBRs to also serve as cladding

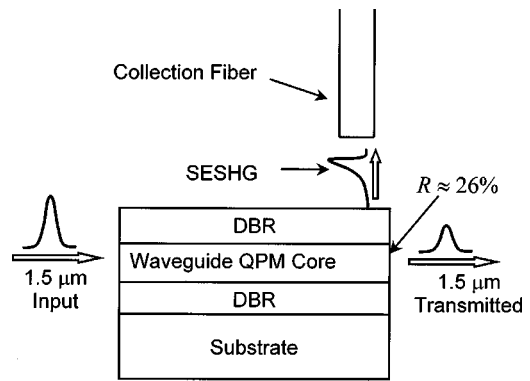


FIG. 2. Rear-facet reflection geometry for characterizing SESHG in the microcavity structure. A portion of the fundamental is reflected at the rear facet, folding the pulse back on itself, thereby creating the required collision geometry. The surface-emitted second harmonic is collected above the waveguide using an optical fiber.

layers, the cavity size is reduced to $5\lambda^{\text{SH}}/2n$, producing a large resonance width and increasing the overlap with the nonenhanced SH spectrum. $\text{Al}_{0.90}\text{Ga}_{0.10}\text{As}$ is used instead of AlAs for the low-index layers in the top DBR to minimize possible oxidation after the strip defining the channel waveguide is etched, exposing these layers to the atmosphere. Note from Eq. (2) that the constructive interference of the two SH components requires positioning of the SH source such that $kl - \phi_b/2$ is an integral multiple of π , which is equivalent to centering the standing wave peaks in the QPM core layers. This is achieved by placing high-index DBR layers ($\text{Al}_{0.45}\text{Ga}_{0.55}\text{As}$) in contact with the top and bottom $\text{Al}_{0.30}\text{Ga}_{0.70}\text{As}$ core layers.

The [211]-oriented AlGaAs structure was grown by molecular-beam epitaxy, and channel waveguides were defined by etching 3 and $4 \mu\text{m}$ wide strips via reactive ion etching. The strips were etched $2.33 \mu\text{m}$ deep, penetrating slightly into the waveguide core layers, and the etched sample was coated with a Si_3N_4 quarter-wave layer via plasma-enhanced chemical-vapor deposition for passivation. A finite-difference beam-propagation technique¹² was used to model the transverse mode profile of the fundamental at the operational wavelength of 1476 nm , resulting in full width at half maximum (FWHM) mode intensities of $0.8 \times 1.5 \mu\text{m}$ for $3 \mu\text{m}$ strips and $0.8 \times 1.7 \mu\text{m}$ for $4 \mu\text{m}$ strips.

SESHG experiments were performed with 200 fs fundamental pulses using a rear-facet reflection geometry (Fig. 2).¹³ A single pulse is launched into the waveguide and allowed to propagate down its entire length. The Fresnel reflection due to the AlGaAs-air interface at the rear facet of the waveguide creates a counter-propagating signal, so that SESHG is produced by the fundamental pulse reflecting back on itself. For accurate efficiency assessment, the fundamental power is determined by measuring the power transmitted through the rear facet. The SESHG signal is collected with a $200 \mu\text{m}$ core optical fiber positioned above the rear facet, and detected with a calibrated Si avalanche photodiode. The effective nonlinear cross section and SESHG spectrum were measured for several waveguides defined by 3 and $4 \mu\text{m}$ strips using a TE-polarized fundamental for optimum SESHG in [211] AlGaAs.

The measured efficiency data is shown in Fig. 3 for mul-

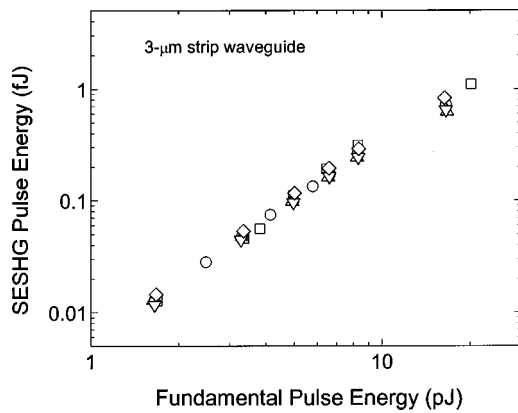


FIG. 3. SESHG efficiency data for a structure with a 2.5 period waveguide core between two AlGaAs DBRs. The channel waveguides are defined by 3 μm strips, and the mode widths used in the A^{NL} calculations are determined by numerical simulation using the measured strip etch depths.

multiple waveguides with a 3 μm strip width. The results are highly uniform among the different waveguides and nearly identical results were obtained from multiple waveguides with 4 μm strip widths. Note that the SH power displays the expected quadratic dependence on pulse energy. The effective nonlinear cross sections for the two different strip widths were calculated using the mode widths obtained via simulation, yielding a value of $\sim 1.6 \times 10^{-6} \text{ W}^{-1}$. In contrast, the maximum theoretical effective nonlinear cross section (neglecting loss) for this structure is $1.4 \times 10^{-5} \text{ W}^{-1}$. We note that this efficiency is sufficient for all-optical demultiplexing of 160 Gb/s optically time-division multiplexed data streams.² Using a loss of $\alpha = 1300 \text{ cm}^{-1}$ yields an enhancement factor of 2.92 and an effective nonlinear cross section of $1.8 \times 10^{-6} \text{ W}^{-1}$, which compares well with the experimental value. We note that this loss may be associated with significant stress-related material degradation that was observed with the [211] structures.

We can separately assess the microcavity loss by comparison of the measured SESHG spectrum and the calculated absorption-broadened spectrum. The measured spectrum exhibits a 2.9 nm width (FWHM), which agrees well with the 2.6 nm width calculated for the microcavity with $\alpha = 1300 \text{ cm}^{-1}$ ($\alpha d \approx 0.07$) as shown in Fig. 4. The width of the nonenhanced SH spectrum, calculated to be $\sim 6 \text{ nm}$, is also shown. It is clearly seen that both the measured SESHG spectrum and the calculated spectrum for $\alpha = 0 \text{ cm}^{-1}$ are indeed significantly narrower than the calculated nonenhanced spectrum, thus demonstrating that significant enhancement is possible for spectral widths not well matched to the microcavity resonance.

We have demonstrated significant enhancement of the SESHG conversion efficiency for 200 fs pulses in AlGaAs QPM waveguides incorporating a vertical microcavity in

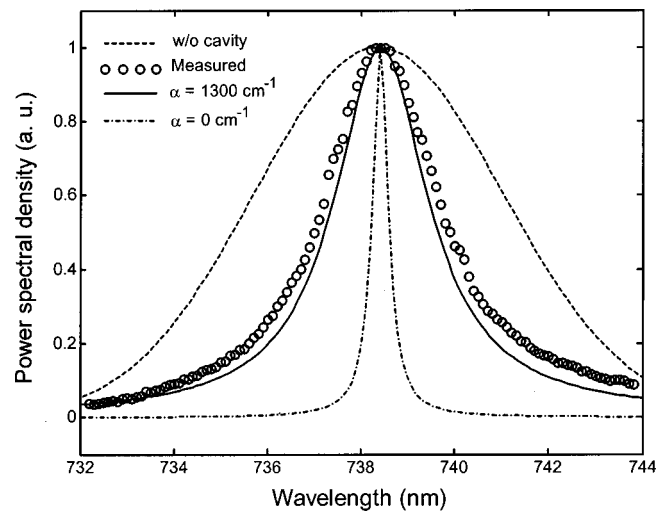


FIG. 4. SESHG spectrum for a 4 μm strip and a $5\lambda^{\text{SH}}/2n$ vertical microcavity. Open circles: experimental data; solid line: calculated spectra with $\alpha = 1300 \text{ cm}^{-1}$; dashed-dotted line: calculated spectra with $\alpha = 0 \text{ cm}^{-1}$; dashed line: calculated spectrum without cavity.

which the cavity resonance is much narrower than the spectral width of the nonenhanced SH. Ultrafast optical time-division demultiplexing with practical input powers may be achieved by reduction of losses, the use of higher index-contrast DBRs (e.g., $\text{Al}_2\text{O}_3/\text{AlGaAs}$)⁵ to reduce the cavity dimension and broaden the resonance, and the use of domain-inverted material.¹⁴

This work is supported in part by BellSouth, Corning, Nortel Networks, and the Georgia Research Alliance.

- ¹R. K. Tan, C. M. Verber, and A. J. SpringThorpe, IEEE Photonics Technol. Lett. **6**, 1228 (1994).
- ²T. G. Ulmer, M. C. Gross, K. M. Patel, J. T. Simmons, P. W. Juodawlkis, B. R. Washburn, W. S. Astar, A. J. SpringThorpe, R. P. Kenan, C. M. Verber, and S. E. Ralph, J. Lightwave Technol. **18**, 1964 (2000).
- ³R. Lodenkamper, M. L. Bortz, M. M. Fejer, K. Bacher, and J. S. Harris, Jr., Opt. Lett. **18**, 1798 (1993).
- ⁴Y. J. Ding, J. B. Khurgin, and S.-J. Lee, J. Opt. Soc. Am. B **12**, 1586 (1995).
- ⁵S. Janz, Y. Beaulieu, A. Fiore, P. Bravetti, V. Berger, E. Rosencher, and J. Nagle, Opt. Express **2**, 462 (1998).
- ⁶D. Vakhshoori and S. Wang, J. Lightwave Technol. **9**, 906 (1991).
- ⁷R. Normandin, H. Dai, S. Janz, F. Chatenoud, C. Fernando, Y. Beaulieu, and A. Delâge, Proc. SPIE **2139**, 296 (1994).
- ⁸P. A. Ramos and E. Towe, Opt. Commun. **132**, 121 (1996).
- ⁹A. Ashkin, G. D. Boyd, and J. M. Dziedzic, IEEE J. Quantum Electron. **2**, 109 (1966).
- ¹⁰D. Vakhshoori, J. Appl. Phys. **70**, 5205 (1991).
- ¹¹I. Shoji, T. Kondo, A. Kitamoto, M. Shirane, and R. Ito, J. Opt. Soc. Am. B **14**, 2268 (1997).
- ¹²BEAMPROP Version 3.0, by RSoft, Inc., Ossining, NY.
- ¹³T. G. Ulmer, R. K. Tan, Z. Zhou, S. E. Ralph, R. P. Kenan, C. M. Verber, and A. J. SpringThorpe, Opt. Lett. **24**, 756 (1999).
- ¹⁴S. Koh, T. Kondo, T. Ishiwada, C. Iwamoto, H. Ichinose, H. Yaguchi, T. Usami, Y. Shiraki, and R. Ito, Jpn. J. Appl. Phys., Part 2 **37**, L1493 (1998).